Biochemical and Structural Characterization of HDAC8 Mutants Associated with Cornelia de Lange Syndrome Spectrum Disorders

Christophe Decroos,[†,‡] Nicolas H. Christianson,[†] Laura E. Gullett,[†] Christine M. Bowman,[†] Karen E. Christianson,[†] Matthew A. Deardorff, [§,¶] and David W. Christianson*[,†,Δ]

[†]Roy and Diana Vagelos Laboratories, Department of Chemistry, University of Pennsylvania, Philadelphia, PA 19104-6323 United States

[§]Division of Human Genetics and Molecular Biology, The Children's Hospital of Philadelphia, Pennsylvania 19104 United States

[¶]Department of Pediatrics, Perelman School of Medicine, University of Pennsylvania, Philadelphia, Pennsylvania 19104 United States

[Δ]Radcliffe Institute for Advanced Study, Harvard University, Cambridge, MA 02138 United States

[‡]Current address: Aix Marseille Université, Centrale Marseille, CNRS, ISM2 UMR 7313, 13397 Marseille, France

*author to whom correspondence should be sent: Tel. (215) 898-5714; E-mail chris@sas.upenn.edu

— SUPPORTING INFORMATION —

DISORDERED RESIDUES IN FINAL MODELS OF HDAC8 MUTANTS

Disordered polypeptide segments excluded from final protein models: G117E HDAC8–TSA complex: M1-S13 (monomers A and B), D87-I94 (monomer A), I378-H389 (monomer A), and E379-H389 (monomer B); D233G-Y306F HDAC8–substrate complex: M1-S13 (monomers A and B), and I378-H389 (monomers A and B); and P91L-Y306F HDAC8–substrate complex: M1-S13 (monomers A and B), D87-P91 (monomer B), I378-H389 (monomer A), and E379-H389 (monomer B). Additionally, Y100 in the L2 loop of the G117E HDAC8–TSA complex (monomer A) is characterized by somewhat ambiguous density; while this residue is included in the final model, it refined with an unfavorable backbone conformation.

Side chains of residues that were partially or completely disordered and excluded from final protein models: G117E HDAC8–TSA complex: L14 (monomer A), R55 (monomer B), K60 (monomers A and B), E65 (monomer A), D73 (monomer A), K81 (monomers A and B), Q84 (monomer B), E85 (monomer A), D88 (monomer B), D89 (monomer B), D92 (monomer B), S93 (monomer B), I94 (monomer B), E106 (monomer B), D110 (monomer B), E117 (monomer B), K168 (monomer A), K221 (monomer B), E238 (monomers A and B), K249 (monomers A and B), E250 (monomer A), Q253 (monomer B), Q293 (monomer B), K325 (monomers A and B), E358 (monomer A), H360 (monomer A), Q364 (monomer A), K370 (monomer B), K374 (monomers A and B), and V377 (monomer B); D233G-Y306F HDAC8–substrate complex: L14 (monomers A and B), K52 (monomers A and B), R55 (monomers A and B), K60 (monomers A and B), E85 (monomer A), D88 (monomer B), D89 (monomer B), K168 (monomer A), K221 (monomers A and B), R223 (monomer B), E238 (monomer A), K249 (monomer B), K370 (monomer A), K374 (monomers A and B), and V377 (monomer B); and P91L-Y306F HDAC8–substrate complex: L14 (monomers A and B), K36 (monomer A), K52 (monomers A and B), R55 (monomers A and B), K60 (monomer A), D73 (monomer B), K81 (monomers A and B), Q84 (monomer A), E85 (monomers A and B), D88 (monomer A), D89 (monomer A), L91 (monomer

A), D92 (monomers A and B), I94 (monomer A), E95 (monomer A), E106 (monomers A and B), E170 (monomer A), K221 (monomer B), E238 (monomer A), K249 (monomers A and B), Q253 (monomers A and B), K258 (monomer B), Q295 (monomer B), K325 (monomer B), E358 (monomer A), Q364 (monomer B), K370 (monomers A and B), K374 (monomers A and B), V377 (monomer B), and I378 (monomer B).

COMPUTER BUILT FOR GROMACS CALCULATIONS

A computer was built to exploit the technologies and efficiencies offered by GROMACS. The quad-core, hyperthreading Intel central processing unit was installed to take advantage of the "thread-MPI" layer included in GROMACS 4.5 and above with its 4 physical and 4 virtual cores, which allows for the use of MPI multithreading, previously available only with supercomputers. Also, the Nvidia GTX 780 graphics processing unit (GPU) was installed to take advantage of the CUDA graphics acceleration routine implemented in GROMACS and VMD (the visualization software used), with 2304 CUDA cores for GPU acceleration. Due to the high thermal output of these two components alone (approximately 500 watts), a liquid cooling system was installed to prevent overheating. The Oculus Rift stereo image headset was adapted for viewing protein structures and MD trajectories in real-time. Benchmark GROMACS calculations demonstrated that the system was about 10 times faster than a quad-core Apple MacBook Pro.

Table S1. Primers used to generate HDAC8 mutants

Mutation		5'-3' sequence
P91L	forward	GC GAT GAT GAT CAT **ctg** GAC TCC ATA GAA TAT GG
	reverse	CC ATA TTC TAT GGA GTC **cag** ATG ATC ATC ATC GC
G117E	forward	CA GCA GCT ATA GGA **gag** GCT ACG ATC ACA GC
	reverse	GC TGT GAT CGT AGC **ctc** TCC TAT AGC TGC TG
H180R	forward	C GTT GAT CTG GAC CTG **cgc** CAC GGT GAT GGT GTT G
	reverse	C AAC ACC ATC ACC GTG **gcg** CAG GTC CAG ATC AAC G
D233G	forward	AT GTG CCC ATT CAG **ggt** GGC ATA CAA GAT GAA
	reverse	TTC ATC TTG TAT GCC **acc** CTG AAT GGG CAC AT
G304R	forward	C CTG ATC CTG GGT GGC **aga** GGT TAC AAC CTG GCG AAC
	reverse	GTT CGC CAG GTT GTA ACC **tct** GCC ACC CAG GAT CAG G
Y306F	forward	GGT GGC GGT GGT **ttt** AAC CTG GCG AAC ACT G
	reverse	C AGT GTT CGC CAG GTT **aaa** ACC ACC GCC ACC

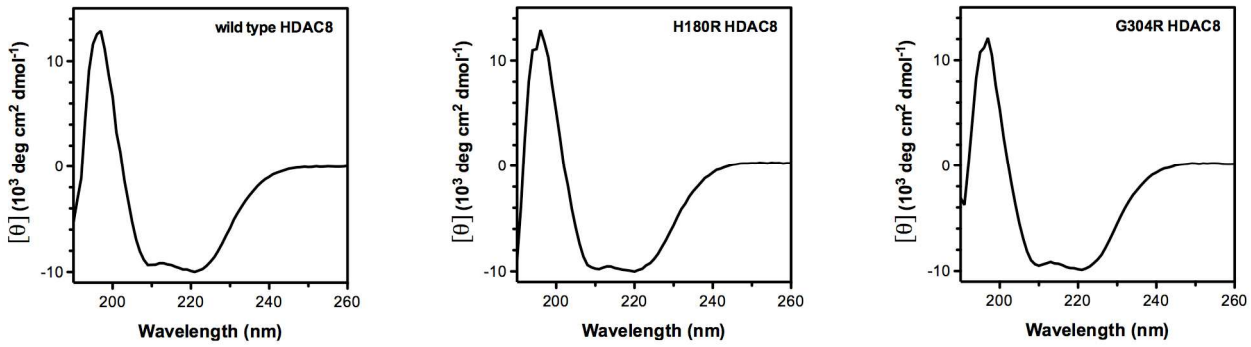

Figure S1. CD spectra measured for wild-type, H180R, and G304R HDAC8 indicate that the mutant enzymes are folded properly and adopt an overall tertiary structure similar to that of the wild-type enzyme.

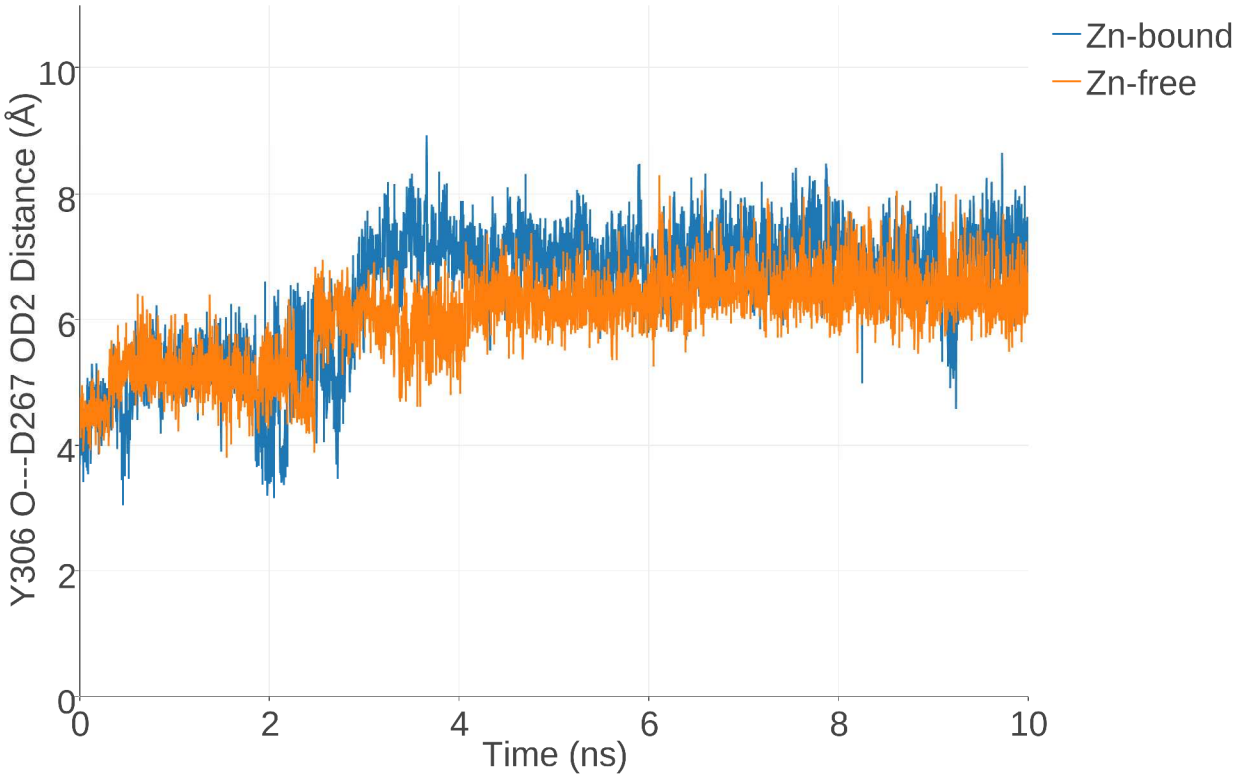

Figure S2. Y306 fluctuates away from the catalytically obligatory "in" conformation slightly less (~1 Å) in Zn^{2+}-free H180R HDAC8 compared with Zn^{2+}-bound H180R HDAC8 over the course of 10-ns MD simulations. To enable comparisons between the Zn^{2+}-free and Zn^{2+}-bound structures, the distance between the Y306 hydroxyl oxygen and the carboxylate oxygen of Zn^{2+} ligand D267 is measured here.

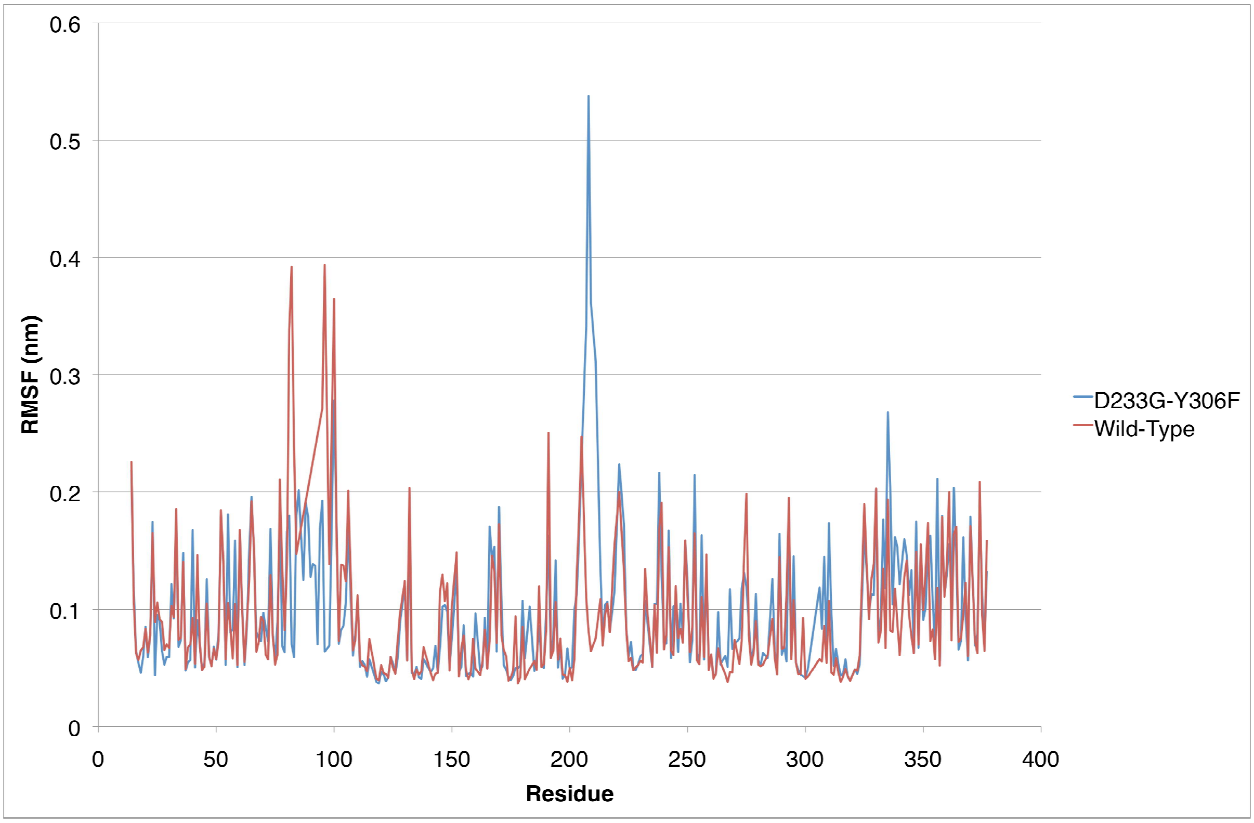

Figure S3. Rms side chain fluctuations of wild-type HDAC8 and D233G-Y306F HDAC8 calculated from 10-ns MD simulations. The D233G mutation triggers notable increases in rms fluctuations for K202 and neighboring residues through F208. Increased atomic fluctuations triggered by the D233G mutation may be consistent with the decreased thermostability measured for this mutant.

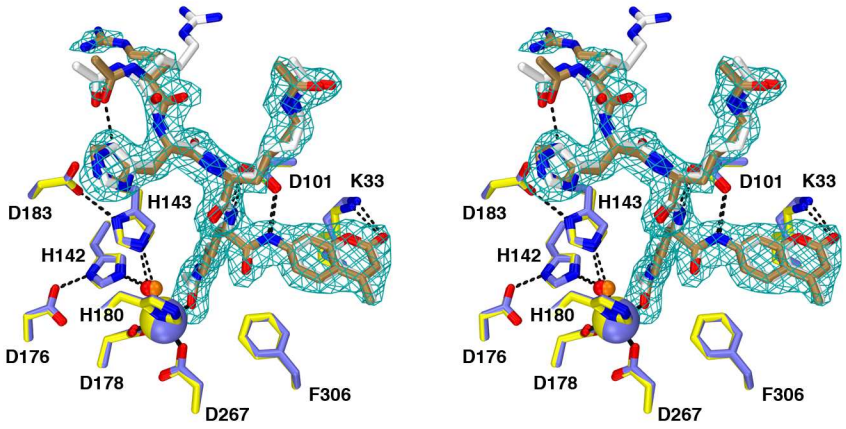

Figure S4. Simulated annealing omit map (contoured at 3.0σ) showing the tetrapeptide substrate bound to the active site of the P91L-Y306F HDAC8–substrate complex (monomer B). Atomic color codes are as follows: C = yellow (protein) or tan (substrate), N = blue, O = red, Zn^{2+} = yellow sphere, water molecule = red sphere. Metal coordination and hydrogen bond interactions are shown as solid black and dashed black lines, respectively. Superimposed is the Y306F HDAC8-substrate complex (C = blue (protein) or gray (substrate), Zn^{2+} = blue sphere, water molecule = orange sphere; PDB accession code 2V5W). The arginine residue of the tetrapeptide substrate in complex with P91L-Y306F HDAC8 appears to be partially disordered and adopts a conformation (in monomer B only) different from that in the Y306F HDAC8-substrate complex structure.